Journal of Alloys and Compounds 1044 (2025) 184617

Contents lists available at ScienceDirect

Journal of Alloys and Compounds

journal homepage: www.elsevier.com/locate/jalcom

Tailoring polarization and dielectric properties in HZO multilayers: Electrostatic Effects vs. structural instabilities

Andra-Georgia Boni [a,*], Polychronis Tsipas [a,b], Dana Popescu [a], Cristian Radu [a], Sara Laafar [a], Lucian Pintilie [a], Athanasios Dimoulas [a,b]

[a] *National Institute of Materials Physics, Atomistilor 405A, Magurele 077125, Romania*

[b] *Institute of Nanoscience and Nanotechnology, National Center for Scientific Research DEMOKRITOS, Neapoleos 27 and Patriarchou Gigoriou Str, Athens, Attiki 15341, Greece*

ARTICLE INFO

Keywords:
Ferroelectric HZO
Electrostatic interactions
Multilayer structures
Dielectric constant enhancement
Polarization switching

ABSTRACT

Ferroelectric hafnium-zirconium oxide (HZO) is a promising material for next-generation electronic devices, particularly suited to addressing the miniaturization and integration challenges of traditional perovskite-structured ferroelectric memory devices. HZO exhibits complex phase competition, requiring careful stabilization to achieve the desired properties. Numerous studies have sought solutions to balance monoclinic, orthorhombic, and tetragonal phases, as their interplay influences the macroscopic ferroelectric and antiferroelectric-like behaviors of the films. While recent research has focused on phase engineering in nanolaminates and multilayers to enhance ferroelectric properties, dielectric constant, and device performance, electrostatic control in multilayers remains less explored. In this study, we systematically investigate how polarization switching and the dielectric constant are affected by electrostatic interactions in multilayer structures. We analyze a wide range of samples beginning with simple layers of varying Hf/Zr compositions and thicknesses, followed by bilayers. Special attention is given to multilayers with alternating HZO compositions and HZO/dielectric (HZO/DE) structures to disentangle the contributions of electrostatic coupling, structural changes, and oxygen vacancy effects. Our findings reveal that electrostatic interactions can enhance the effective dielectric constant in multilayers, with significant amplification observed in HZO(30/70)_HZO(50/50) with 5 nm/5 nm thickness and ZrO_2_HZO(50/50) with 7 nm/7 nm thickness structures compared with simple layers. For multilayers where amplification is not observed, the main limiting factors are the coexistence of non-polar phases or a lack of control between FE and AFE-like characteristics. These results provide key insights into tailoring the dielectric response of HZO-based thin films and improving their ferroelectric performance. Electrostatic control is a clear pathway for tuning specific properties and enabling new potential applications. However, their effects can be weakened or misinterpreted without precise control over the phase ratio in HZO. Future research should refine processing conditions to achieve better phase control and enhance the stability of HZO-based materials for advanced electronic applications.

1. Introduction

Since the groundbreaking discovery of ferroelectricity in 10 nm thick Si doped HZO films [1], HZO-based materials have emerged as promising candidates for next-generation high-density non-volatile memory technologies. These materials are particularly suited to address the miniaturization and integration challenges faced by traditional perovskite-structured ferroelectric memory devices, drawing significant attention from both academia and industry. HfO2 is already widely used as a isolator material in semiconductor processes, and its dielectric properties have been extensively studied. Various approaches have been employed to control its ferroelectric, antiferroelectric-like, and dielectric properties, including different deposition techniques, element doping, the use of morphotropic phase boundaries (MPB), and the creation of nanolaminates or superlattices [2–7].

Ferroelectric HZO is particularly difficult to obtain in a single phase, even when using epitaxial deposition techniques. In many cases, it is deposited in an amorphous state and then requires annealing under

* Corresponding author.
E-mail address: andra.boni@infim.ro (A.-G. Boni).

https://doi.org/10.1016/j.jallcom.2025.184617
Received 20 May 2025; Received in revised form 19 October 2025; Accepted 22 October 2025
Available online 24 October 2025
0925-8388/© 2025 The Authors. Published by Elsevier B.V. This is an open access article under the CC BY license (http://creativecommons.org/licenses/by/4.0/).

specific conditions to induce crystallization.

The stabilization of the ferroelectric phase in HZO is quite complex and has remained an active research topic for many years. The stable phase of HZO is monoclinic, but as DFT calculations and many experiments have shown, an orthorhombic ferroelectric phase can be stabilized under certain conditions [8]. Additionally, the occurrence of antiferroelectric-like characteristics has been extensively investigated. It is now widely accepted that the low-energy stable state of ZrO_2 is tetragonal, which also holds true for ZrO_2-rich compositions of HZO. This nonpolar centrosymmetric phase can undergo a field-induced transformation into a ferroelectric phase. Therefore, this antiferroelectric-like behavior is now often considered a case of field-induced ferroelectricity (FFE) [8–10].

Many previous studies have shown how the concentration range [11–13], dopant type [9,14,15], and field cycling effects impact the establishment of different phases, the coexistence of phase mixtures, and their interplay in the macroscopic ferroelectric response of the films. The main conclusions indicate that different phases seem to coexist, being close in energy, making the system rich in competing phenomena. Thus, extensive research has been conducted on stabilizing a significant volume of the sample in the orthorhombic or tetragonal phase, using various deposition techniques, dopants, substrates, and electrodes.

In recent years, numerous studies have explored the engineering of nanolaminates based on HZO layers [16–21], inspired by research on perovskite ferroelectric superlattices [22–24]. The purpose of these studies has been to enhance ferroelectric characteristics such as remanent polarization, lower coercivity, and improved endurance under fatigue cycles, as well as to achieve a higher dielectric constant. The dielectric constant of HfO_2-based ferroelectric thin films is a critical factor influencing the performance of semiconductor memory devices, including ferroelectric field-effect transistors (FeFETs), ferroelectric random-access memories (FeRAMs), and ferroelectric tunnel junctions (FTJs). An increased dielectric constant can effectively reduce the subthreshold swing (SS) value and the equivalent oxide thickness (EOT) in HfO_2-based FeFETs, for example. Although HZO is considered a high-k material, its dielectric constant is not comparable to that of ferroelectric perovskites. Most studies on nanolaminates and superlattices based on HfO_2 focus on the relationship between structural control—specifically, the modification of different phases (monoclinic, orthorhombic, and tetragonal)—and changes in electrical characteristics. Many studies report various strategies to control the phase ratio and the possibility of obtaining a morphotropic phase with an enhanced dielectric constant [3,25,26]. Previous work [3] revealed that HfO_2–ZrO_2 nanolaminates engineered to exploit a morphotropic phase boundary (MPB) can achieve dielectric constants up to $\varepsilon_r \approx 60$, owing to the coexistence of ferroelectric and antiferroelectric phases at the nanoscale. Similarly in [25] Cheema et al. demonstrated that ultrathin HfO_2–ZrO_2 superlattices with mixed ferroic ordering, integrated directly on Si transistors, enable drastically reduced EOT (~6.5 Å) and enhanced capacitance without sacrificing leakage or mobility. In general, dielectric constant engineering (ε-engineering) in HfO_2-based systems is often achieved via the formation of a morphotropic phase boundary (MPB) [27,28].

Besides the successful control of ferroelectric (FE) and dielectric (DE) properties in nanolaminates and superlattices—primarily achieved through precise structural phase control in HZO—another aspect remains less explored compared to perovskites: electrostatic control in multilayers. As the structure transitions from very thin superlattices -epitaxial heterostructures with a well-defined periodic repetition of layers, atomically sharp and coherent interfaces, and strong interlayer coupling -to nanolaminates and then to thicker multilayers -artificial stacks of layers in the nanometer range without the need for coherent epitaxy or long-range periodicity -electrostatic interactions become increasingly significant. These interactions can lead to different electrostatic couplings, potentially giving rise to atypical phenomena. For example, such effects could enable sequential polarization switching [29–32], controlled imprint engineering to modulate the negative regime during switching [33,34], the achievement of extremely high energy storage densities [35–37], or the stabilization of negative capacitance (NC) in multilayers. However, these phenomena remain largely unexplored in both perovskite-based and HZO-based systems, leaving open questions about their fundamental mechanisms and potential applications [38–40].

This study aims to explore the electrostatic control of polarization switching and dielectric properties in multilayer HZO thin films. To achieve this, we first evaluate the ferroelectric and dielectric properties of simple HZO thin films with an Hf/Zr ratio of 50/50 (denoted HZO(50/50)) at different thicknesses, as well as Zr-rich HZO with an Hf/Zr ratio of 30/70 (denoted HZO(30/70)), which serves as a reference point for multilayers. Next, we analyze the properties of multilayer structures with different configurations: (i) ferroelectric bilayers with varying Hf/Zr ratios and (ii) FE/DE structures, where an HZO(50/50) layer serves as the ferroelectric (FE) component and TiO_2 or ZrO_2 is used as the dielectric (DE) component. By designing these structures with tailored polarization values in the constituent layers, we investigate the conditions that influence the ferroelectric and dielectric properties. The primary objective is to control the electrostatic internal fields in multilayers, a particularly challenging task in HZO-based systems compared to perovskites. This difficulty arises due to significant challenges related to phase stability and defect formation in HZO multilayers. Here, *structural instabilities* refer to the competition and coexistence between monoclinic, orthorhombic, and tetragonal phases, which are close in energy and can be easily influenced by external factors such as stress, electric field, or interface effects Fig. 1.

2. Theory

If we consider the electrostatic properties of a system formed by two ferroelectric layers in contact, with similar properties but a small difference in polarization values, the distribution of electric fields and the stabilization of different polarization states in the ferroelectric layers correspond to the following electrostatic requirements:

Kirchhoff's voltage law:

$$V_{app} = V_1 + V_2 \tag{1}$$

Where, $\boldsymbol{V_{app}}$ is the total applied voltage across the two-layer structure, V_1 and V_2 are the voltage drops across layer 1 and layer 2, respectively.

Constant flux density/ continuity of the displacement vector at the interface: $D_1 = D_2$

$$\varepsilon_1 \varepsilon_0 E_1 + P_1 = \varepsilon_2 \varepsilon_0 E_2 + P_2 \tag{2}$$

Where, ε_1 , ε_2 are the relative permittivity of layer 1 and layer 2, ε_0 is the vacuum permittivity, E_1, E_2 are the electric fields in layer 1 and layer 2, respectively, P_1, P_2 are the polarization vectors in each layer, D_1, D_2 are the total electric displacement vectors in the respective layers.

This situation corresponds to an ideal case, where no other electrostatic or structural effects are involved, but in real situations, factors like

Fig. 1. Schematic representation of the configuration of the simple layers and of the multilayers used.

finite conductivity in each ferroelectric layer and the properties of any isolator interface can significantly affect the structure's electric behavior.

If the two ferroelectric layers have similar values for P_1 and P_2, no significant internal fields will appear when $V = 0$, or the switching will be very similar to the switching of the constituent layers. If the polarization of the two layers is different, non-zero internal fields will appear, even if $V_{app} = 0$ and Considering also the relation between electric field and voltage, and assuming uniform fields and thicknesses normalized in terms of capacitances:

$$V_1 = \frac{P_2 - P_1}{(C_1 + C_2)} \text{and} V_2 = -\frac{P_2 - P_1}{(C_1 + C_2)}. \quad (3)$$

Where $C_1 = \frac{\varepsilon_1 \varepsilon_0}{t_1}$ and $C_2 = \frac{\varepsilon_2 \varepsilon_0}{t_2}$ are the capacitances per unit area of each layer (assuming planar geometry), t_1 and t_2 are the thicknesses of layers 1 and 2.

One of these internal fields will align with the polarization direction in that layer, while the other will be oriented oppositely to the polarization as schematically represented in Fig. 2a). This electrostatic condition forces the ferroelectric layers into polarization states that would be unstable under normal conditions if the layers were standalone systems. With careful structural design, these internal fields can be engineered to reach magnitudes comparable to the coercive fields. In the layer where the electric field is oriented opposite to the polarization, this condition can drive the ferroelectric material into a negative capacitance state (Fig. 2b), by placing the system in the concave region of the free energy landscape, which corresponds to the negative capacitance (NC) regime. Even if a negative capacitance state is not achieved, the large variation of the capacitance as function of polarization suggests that an enhancement of the effective dielectric constant is expected in the layer where the polarization and internal field are antiparallel (Fig. 2b)).

If one of the previously considered ferroelectric (FE) layers has very low polarization, is in a paraelectric state, or acts simply as a dielectric, a large polarization difference can develop within the ferroelectric, leading to an internal field that opposes the polarization. As a result, very strong internal fields are induced in these structures [41]. If these internal fields act as depolarization fields, different compensation mechanisms may occur during processing, such as domain formation, in-plane domain formation [42,43], defect generation, and increased leakage currents [44–47]. Consequently, the macroscopic polarization may be significantly reduced, and the electrostatic conditions required for NC stabilization are not fulfilled. As a result, the observation of NC in FE/DE structures is rare and typically occurs very close to the phase transition in perovskites, such as in PZT/STO superlattices [48] or BTO/STO multilayers [38–40].

Even though the polarization in HZO is quite similar to that of ferroelectric BTO, the depolarization fields in HZO remain relatively large due to its low dielectric constant. By constructing HZO/DE structures or bilayers with different Hf/Zr ratios, we expect only small variations in the numerator of Eq. 3. By adjusting the layer thicknesses, the capacitance ratio can be engineered so that the internal electric fields approach the coercive field, facilitating enhanced electrostatic control and stabilization of the system in a regime with increased capacitance.

3. Experimental details

HZO thin films were grown by plasma-assisted molecular beam epitaxy (MBE) on p-type Ge(100) substrates with resistivity of 0.013 Ω cm. Ge substrates were annealed at 450 °C for several minutes prior to deposition until a clean, 2 × 1 reconstructed, Ge surface appeared. Subsequently, HZO films were deposited at the low substrate temperature of 120°C by co-evaporating Hf and Zr from e-gun evaporators using a remote RF plasma source at 350 W and O_2 partial pressure of 7.5×10^{-6} Torr to produce HZO in the amorphous state as evidenced by

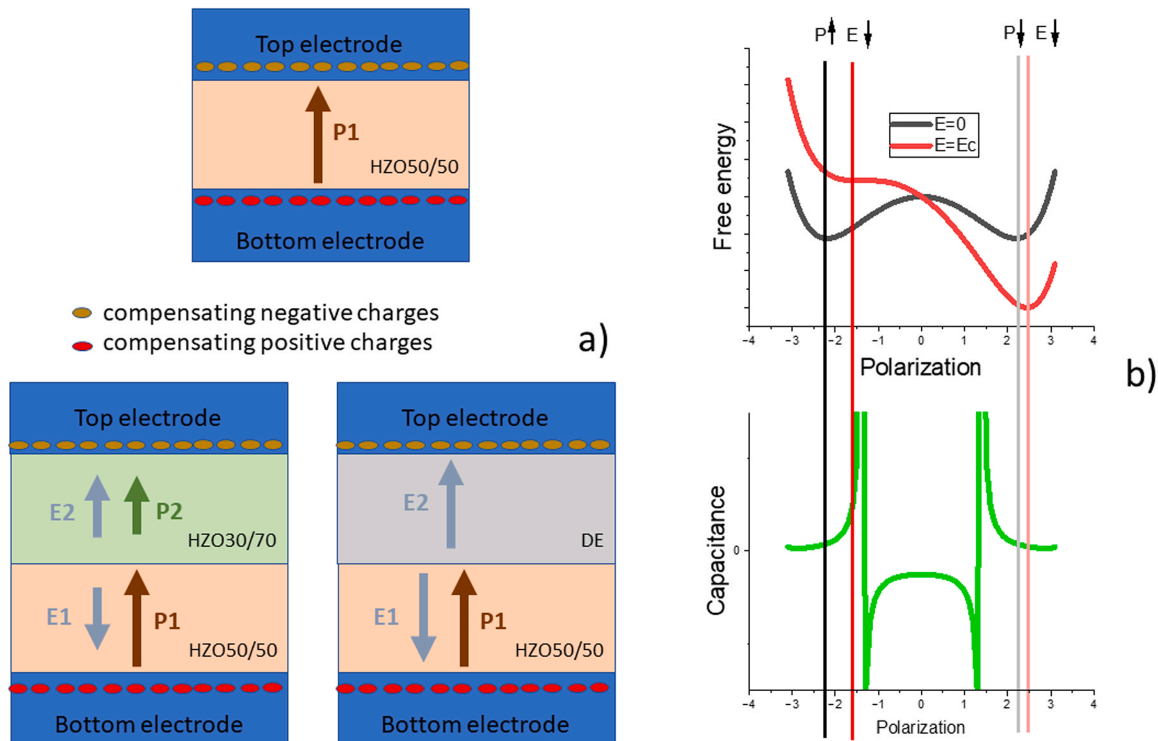

Fig. 2. a) Schematic representation of the distribution of polarization and internal fields in an FE1/FE2 system and in an FE/DE system. b) Representation of the free energy as a function of polarization, both without an applied electric field and with an electric field around the coercive value. Also shown is the dependence of the effective capacitance on the polarization states. The black and red lines indicate the minima of the free energy, corresponding to stabilized polarization states, and illustrate the connection between these states and the changes in the effective dielectric constant/capacitance between stable states at zero applied field and near coercivity.

reflection high-energy electron diffraction (RHEED). A thickness monitor was used in order to control the evaporation rate of Hf and Zr at the nominal values to obtain the required compositions. The compositional ratio of Hf/Zr can be calculated by the Hf4f and Zr3d X-ray photoelectron spectroscopy (XPS) spectra using the relation $C_{Hf}/C_{Zr} = (A_{Hf}/S_{Hf})/(A_{Zr}/S_{Zr})$ where C_{Hf}, C_{Zr} are the atomic concentrations, A_{Hf}, A_{Zr} are the spectral area and SHf4f~ 2.10 and SZr3d~2.05 the XPS sensitivity factors for hafnium 4 f and zirconium 3d core levels. The HZO samples were cut into two equal pieces. In one half piece, a 10-nm-thick TiN metal was grown on top of HZO films without breaking vacuum at the same temperature with an evaporation Ti rate of 0.1 Å/s and rf nitrogen plasma at 350 W. The second piece was left as it was. After TiN growth, both samples (Ge/HZO/TiN and Ge/HZO) received a rapid thermal annealing (RTA) at 420°C for 400 sec in N_2 atmosphere and a ramp-up of 150°C. To fabricate the metal-ferroelectric-semiconductor (MFS) capacitors, Ti(5 nm)/Pt(40 nm) metal contacts were deposited on both Ge/HZO/TiN and Ge/HZO structures by photolithography. Finally, in the case of Ge/HZO/TiN/Ti/Pt structures, the TiN layer was selectively etched by $NH_4OH/H_2O_2/H_2O$ solution to finalize the Ge MFS capacitor.

The X-ray diffraction patterns were recorded with a Rigaku SmartLab-3 kW system (Rigaku Corporation, Tokyo, Japan), equipped with an X-ray tube with a copper anode powered at 40 kV and 40 mA. We worked with the Cu Ka1 radiation (λ = 1.5406 Å) selected from the incident beam by using a Parallel Beam geometry to address the crystalline status/phase composition of the polycrystalline films. GIXRD patterns were recorded at room temperature over 2θ range 24–70°, with a step of 0.04°, with a recording speed of 0.5 gpm, using a 0D detector in grazing incidence (ω=0.5°).

High-resolution transmission electron microscopy (HR-TEM) was performed using a JEM-ARM 200 F microscope (JEOL, Tokyo, Japan) to investigate the microstructural features of the samples at the atomic scale. The cross-section TEM specimen was prepared, for TEM analysis, by mechanical polishing down to cca. 30 μm, followed by ion milling in a Gatan PIPS machine at 4 kV accelerating voltage and 7° incidence angle. Low-voltage ion milling was used as a final polishing stage in order to reduce the amorphous surface layer enveloping the specimen

The electrical properties of the samples were investigated using a LakeShore CPX-VF probe station. Polarization–electric field (P–E) and current–voltage (I–V) hysteresis loops were measured using a TF Analyzer 2000 ferroelectric tester at a pulse frequency of 1 kHz. The samples are wake-up-free [49], showing clear ferroelectric switching from the first measurement cycles. The pulse amplitude was increased stepwise to approach polarization saturation while avoiding electrical degradation. Capacitance–voltage characteristics and impedance spectroscopy measurements were carried out using a HIOKI-50 LCR Hi-Tester.

4. Results

The equilibrium nonpolar monoclinic ($P2_1/c$) and nonequilibrium tetragonal ($P4_2/nmc$) phases are most frequently observed to coexist with the nonequilibrium ferroelectric polar orthorhombic phase in HfO_2 thin films [50–52], Meanwhile, recent studies have shown that electric field cycling can cause a phase transition from the antipolar orthorhombic phase (*Pbca*) to the polar orthorhombic ($Pca2_1$) phase [53] This suggests that the antipolar orthorhombic phase, which is frequently disregarded, may be an important phase impurity that affects ferroelectric performance and shapes the wake-up behavior seen in HfO_2-based thin films. Monoclinic ($P2_1/c$), tetragonal ($P4_2/nmc$), antipolar (*Pbca*), and polar ($Pca2_1$) orthorhombic phases all interact in a way that is unavoidably complex and influenced by a number of variables, such as dopant/substituent type and concentration [54,55] stress [56,57], oxygen vacancies [58], and film thickness or grain size. It is challenging and essential to separate the interaction of these conflicting effects, and doing so calls for precise phase identification in thin films, which are normally less than 30 nm thick [59]. However, phase identification in hafnia thin films is not simple. The phases found in HfO_2-based thin films are frequently evaluated using grazing-incidence X-ray diffraction (GIXRD) because of its relatively high throughput, non-destructive nature, and surface sensitivity.

The diffraction patterns for the simple layers and bilayers structures are displayed in Fig. 3, where a mixture of the polar orthorhombic (i.e., ferroelectric, $Pca2_1$), antipolar orthorhombic (*Pbca* – PDF 01–083–0808), and tetragonal ($P4_2/nmc$ – PDF 04–014–0991) phases can be linked to the dominant signature seen around 30.5°. Although they are present, the monoclinic phase ($P2_1/a$ – PDF 00–034–0104) signatures are significantly less pronounced, with the exception of HZO (50/50)/HZO(30/70) samples with 7 nm/7 nm thikness. For instance, the ($\bar{1}11$) and (111) monoclinic reflections are indexed as the two maxima at 28.3 ° and 31.6 °, respectively. Because the *d*-spacings of the orthorhombic and tetragonal phases are comparable, this peak is difficult to index; thus, it may be the consequence of the tetragonal (101) reflection, the orthorhombic (111) and (211) reflection, or a superposition of the three reflections. [60]. They are referred to as o-(111)/t-(101) in this context. By characterizing their electrical properties, these phases can be distinguished from one another. The tetragonal phase will respond like an antiferroelectric, while the orthorhombic phase will exhibit polarization hysteresis. The patterns were fitted using FullProf software, considering only the orthorhombic (*Pbca*), tetragonal ($P4_2/nmc$), and monoclinic ($P2_1/a$) space groups as a visual guide.

The HZO(50/50) with 14 nm thickness, HZO(50/50)_HZO(30/70) with 7 nm/7 nm thickness and TiO_2/HZO(50/50) samples exhibit low intensity monoclinic phase peaks, whereas the HZO(50/50) with 7 nm thickness, HZO(30/70) and the other multilayers samples do not. The film containing HZO(30/70)/ HZO(50/50)_7 nm/7nm also featured peaks that were indexed as the monoclinic phase, but of higher intensity, in addition to the orthorhombic and/or tetragonal phases.

Particularly, the HZO(30/70)/HZO(50/50) and HZO(50/50)/HZO (30/70) bilayers (7 nm/7 nm) present different monoclinic fractions depending on the deposition sequence: the monoclinic reflections are stronger when HZO(30/70) is the bottom layer. We tentatively attribute this asymmetry to sequence-dependent crystallization pathways during post-deposition annealing. When HZO(30/70) (AFE-like, centrosymmetric) is deposited first, the top HZO(50/50) crystallizes on an insulating underlayer rather than directly on the conductive Ge electrode; the reduced electrical screening enhances the depolarizing field during nucleation and growth, favoring stabilization of the non-polar monoclinic phase at the expense of the polar orthorhombic phase. Conversely, with HZO(50/50) at the bottom (in contact with Ge), improved charge compensation during crystallization promotes the orthorhombic phase and thus lowers the monoclinic fraction.

In Fig. 4 is presented the TEM image at low magnification in diffraction contrast for HZO(50/50)_HZO(30/70)_7 nm/7nm in a) and for TiO_2/HZO(50/50) in b). The measured thickness of the HZO layer is 15–16 nm in the first case and 13–14 nm for HZO and 6–7 nm for TiO_2 in the second case. It can be observed that films are continuous with no variation of the thickness along the entire images. The SAED pattern (insets) corresponds to an area which contains both the HZO layer and the Ge substrate. The brightest spots are assignerd to the Ge substrate oriented with the [001] axis parallel to the surface normal and oriented in the [-110] zone axis. Spots that correspond to the (111) lattice planes with d= 0.282 nm interplanar distance and (11−1) planes with an interplanar distance of 0.315 nm of the monoclinic HZO structure were observed in the diffraction patternin in the first case. The marked diffraction spots correspond to the (111) orthorombic HZO planes were measures at d_{111}= 2.96 A thus confirming the presence of the phase in the case of TiO_2/HZO(50/50).

In the higher magnification HRTEM images presented in Fig. 5 one can observe the lack of a clear boundary between the two HZO layers:

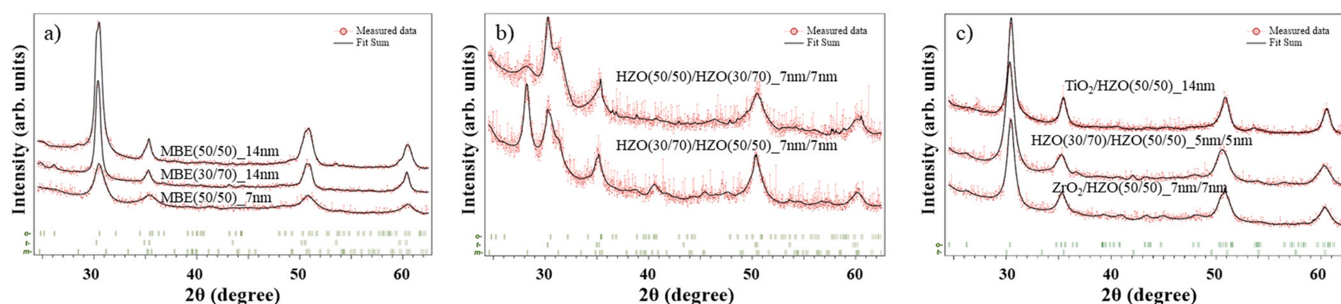

Fig. 3. GIXRD patterns of the a) simple thin films of HZO(50/50) with 7 nm and 14 nm thickness and for HZO(30/70); b) HZO(50/50)/HZO(30/70) and HZO(30/70)/HZO(50/50) with 7 nm/7 nm thickness; c) HZO(30/70)/HZO(50/50) with 5 nm/5 nm and ZrO_2/HZO(50/50) with 7 nm/7 nm thickness; d) TiO_2/HZO(50/50); having orthorhombic/tetragonal, and monoclinic phases (as can be seen from the green bars), with the fits performed using the FullProf software as a visual guide (black lines).

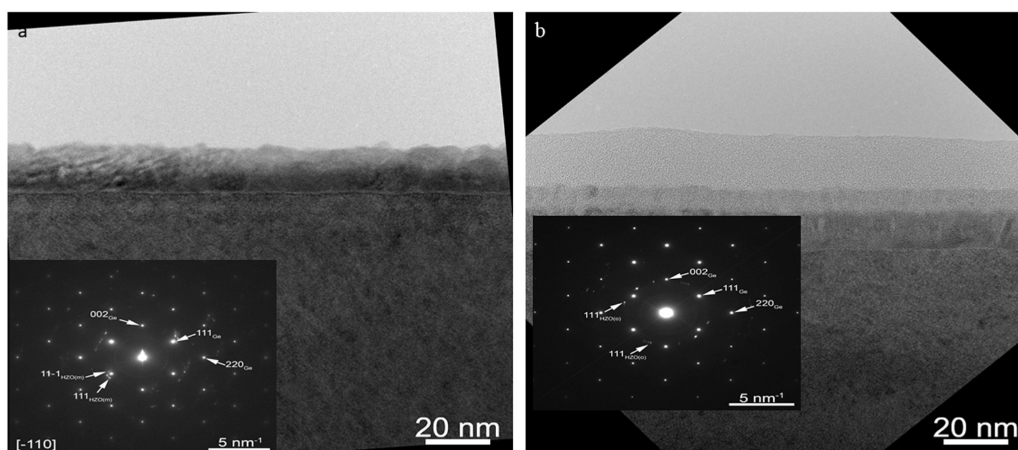

Fig. 4. Low magnification TEM image of the HZO/Ge structurea and, with the inset the corresponding SAED pattern of a region containing both the thin film and the substrate, for a) HfZrO3(50/50)/HfZrO3(30/70) and for b) HfZrO3(30/70)/HfZrO3(50/750) for 7 nm/7 nm thickness.

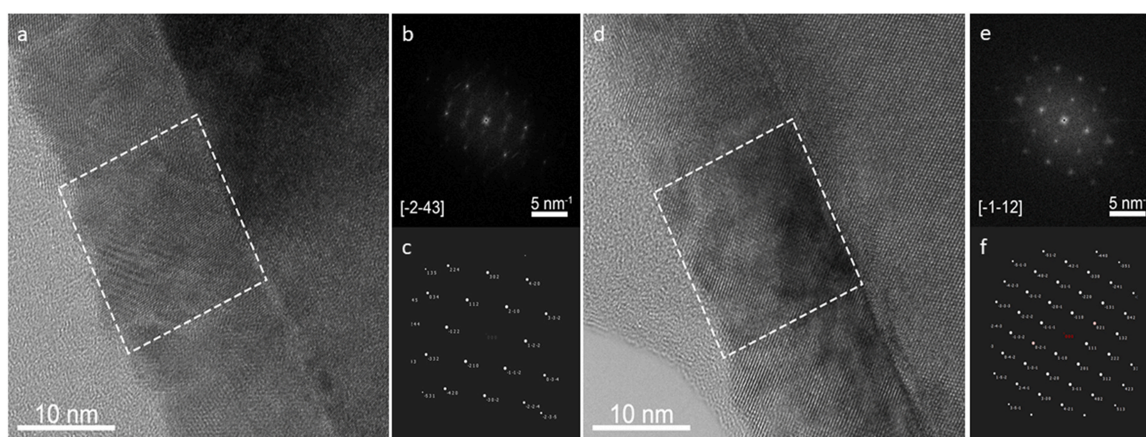

Fig. 5. (a) HRTEM image of the HZO(50/50)_HfZrO3(30/70)_7 nm/7nm structure. (b) FFT pattern corresponding to the marked area in (a), (c) Simulation of the diffraction pattern of HZO(m) oriented along [-2−43] zone axis. (d) HRTEM image of the HZO layer (e) FFT pattern corresponding to the marked area in (d), (f) Simulation of the diffraction pattern of HZO(o) oriented along [-1−12] zone axis.

HZO(50/50)_HZO(30/70)_7 nm/7 nm, and single grain regions are spanning the whole film thickness from the substrate to the surface.

The identification of the HZO phase present in the sample was performed using the Fourier analysis technique. In Fig. 5a FFT analysis of a crystalline region of the HZO film was performed for HZO(50/50)_HZO(30/70)_7nm/7nm. The Fourier image (Fig. 5b,e) corresponds to the area marked in Fig. 3a respectively Fig. 3d. The observed spots form a pattern that can be attributed to the monoclinic phase of HZO oriented along the [-1−22] zone axis and is in good agreement with the single crystal diffraction simulation (Fig. 3c). Fig. 3d. displays a low magnification TEM image of HZO layer and the corresponding SAED pattern taken on another region of the specimen. From the SAED pattern we can observe a different orientation of the substrate (the zone axis is along the [-3−10] direction). The brightest spots are assignerd to the Ge substrate

oriented with the [001] axis parallel to the surface normal. Spots belonging to the (111) interplanar distance (d_{111}=0.296 nm) of the orthorombic HZO phase (space group Pca21 or Pbcm) have been measured.

Fig. 6a presents an HRTEM image for TiO_2/HZO(50/50) overlapped with the filtered images corresponding to the substrate (blue), and two HZO(o) crystallites. The image was obtained by masking out the indicated spots from the FFT pattern and then performing the inverse transform. The spots marked pointed with red and green belong to the (111)HZO(o) lattice planes of two different crystallites. There is a small angular separation of 2^0 between the (111) planes of the two crystallites.

The characterization of switching was performed by applying a series of PUND pulses: after a poling pulse, two consecutive pulses with the same amplitude and polarity are applied, followed by two additional pulses with the opposite polarity. These pulse sequences are specifically used to highlight the differences between the switching and non-switching components in high-speed current/voltage or polarization/voltage characteristics. From these measurements, the remnant current/voltage or polarization can be extracted by making the difference between the two pulses with the same polarity. The four-pulse measurement result is presented in Supplementary Material Figure S1, while Fig. 7 shows the extracted remnant polarization for the two HZO(50/50) thicknesses and the dynamic hysteresis for AFE-like HZO(30/70).

For the HZO(50/50) samples with thicknesses of 14 nm and 7 nm, and for HZO(30/70) with a thickness of 14 nm, the ferroelectric or antiferroelectric character is easily observed, as shown in Fig. 7. The PUND pulse is particularly useful for isolating a small dielectric or leakage contribution. HZO(30/70) exhibits an antiferroelectric-like (AFE) hysteresis that saturates at voltages above 6 V. The remnant polarization in this case is very small, less than 5 μC/cm^2. HZO(50/50) with varying thicknesses shows a ferroelectric (FE) hysteresis loop. The thinner HZO(50/50) sample displays an almost rectangular hysteresis loop, with a very high remnant polarization of nearly 25 μC/cm^2, and a high coercive voltage; the polarization saturation is incomplete up to 4.5 V, which is the maximum applied voltage before breakdown.

In the case of the 14 nm HZO(50/50) sample, polarization switching appears to occur in two steps, resulting in a remnant polarization of 15 μC/cm^2. These differences in behavior between thicknesses for HZO (50/50) are likely correlated with structural differences, where in thinner samples, the non-ferroelectric monoclinic phase is absent.

The remnant hysteresis results for the multilayers are presented in Fig. 8. The PUND characteristics are particularly useful in these situations for highlighting the switching and remnant polarization (Figure S2). For instance, in the case of HZO multilayers, the switching is less sharp than in single layers, and polarization saturation is not achieved within the voltage range that avoids breakdown.

- For the 5 nm/5 nm sample, a higher polarization saturation is achieved compared to thicker structures. However, this increased saturation is accompanied by a significant imprint shift toward positive voltages. The remnant polarization reaches approximately 5 μC/cm^2, while the switching process is less abrupt than in single-layer structures.
- When the HZO(30/70) layer is replaced with a ZrO_2 layer in a 7 nm/7 nm multilayer configuration, the hysteresis characteristics show a higher saturated and remnant polarization, which exceeds 5 μC/cm^2. This configuration also reveals a large internal field oriented toward negative voltages, and a broader switching current peak for positive voltages. Similar to the 5 nm/5 nm structure, polarization saturation is not fully achieved.
- For the structure where a thin TiO_2 layer is deposited on top of a 14 nm HZO(50/50) layer, a different switching behavior is observed. Compared to the single-layer HZO(50/50), the coercive voltages are higher, and the switching peaks are broader. However, the remnant polarization remains similar to that of the single-layer structure, around 15 μC/cm^2. A slight imprint shift toward negative voltages is also noted, which is consistent with the behavior observed in both the 5 nm/5 nm and ZrO_2_HZO multilayer configurations.
- For the HZO(50/50)_HZO(30/70) multilayer structures with 7 nm/7 nm layers, the remnant polarization varies between 2 and 4 μC/cm^2, depending on the deposition order of the layers. The switching peaks are much broader, and the coercive voltages are higher than those observed in single layers. Polarization saturation is not achieved within the same voltage range as in single layers of similar thickness or in other multilayers with comparable thickness.

The capacitance-frequency measurements for the single layers are shown in Figure S3. To compare the dielectric properties of the analyzed HZO-based structures, it is essential to normalize the measurements. Since capacitance is dependent on the thickness of the sample, it is reasonable to extract a dielectric constant using the parallel plate capacitor formula as it is represented in Fig. 9. Additionally, a correction is required due to a series capacitance that arises from various factors (semiconductor region near the interface, interface defect charging, dead layer) and which has been previously deduced for simple HZO layers deposited under the same conditions to be around 6 μF cm^{-2} [49]. The obtained dielectric constant for HZO(50/50) of 14 nm at 1 kHz is about 42 which is in good agreement with previous study [49]. The deduced values for the case of HZO(50/50) of 7 nm are quite low, about 20 at 1 kHz, which are also not aligned with many previous

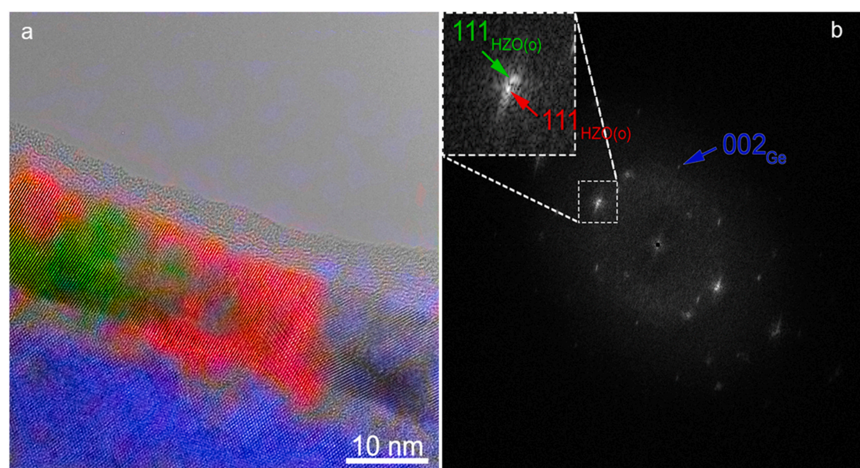

Fig. 6. (a) HRTEM image of the TiO_2/HZO(50/50) overlaid with the images obtained by masking the FFT spots marked from the pattern in (b) which corresponds to the entire image (a).

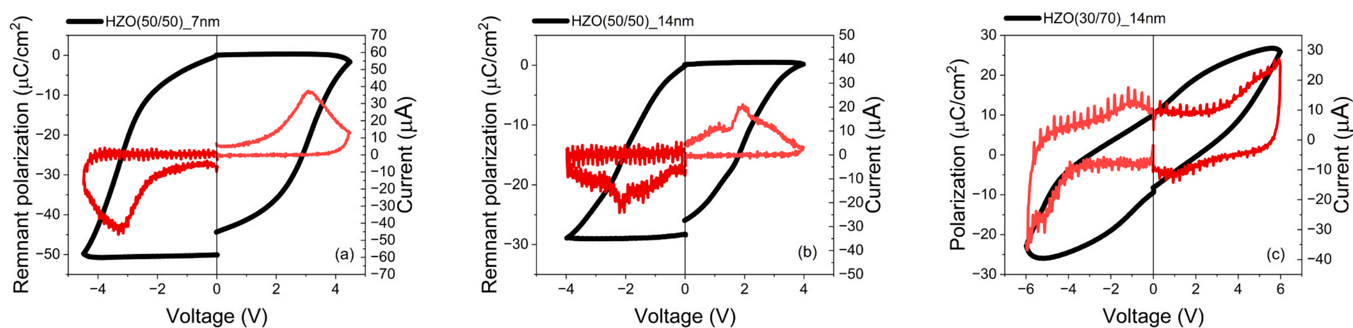

Fig. 7. The remnant polarization and current-voltage hysteresis cycles for a) HZO(50/50)_7nm; b) HZO(50/50)_14nm and c) HZO(30/70)_14nn.

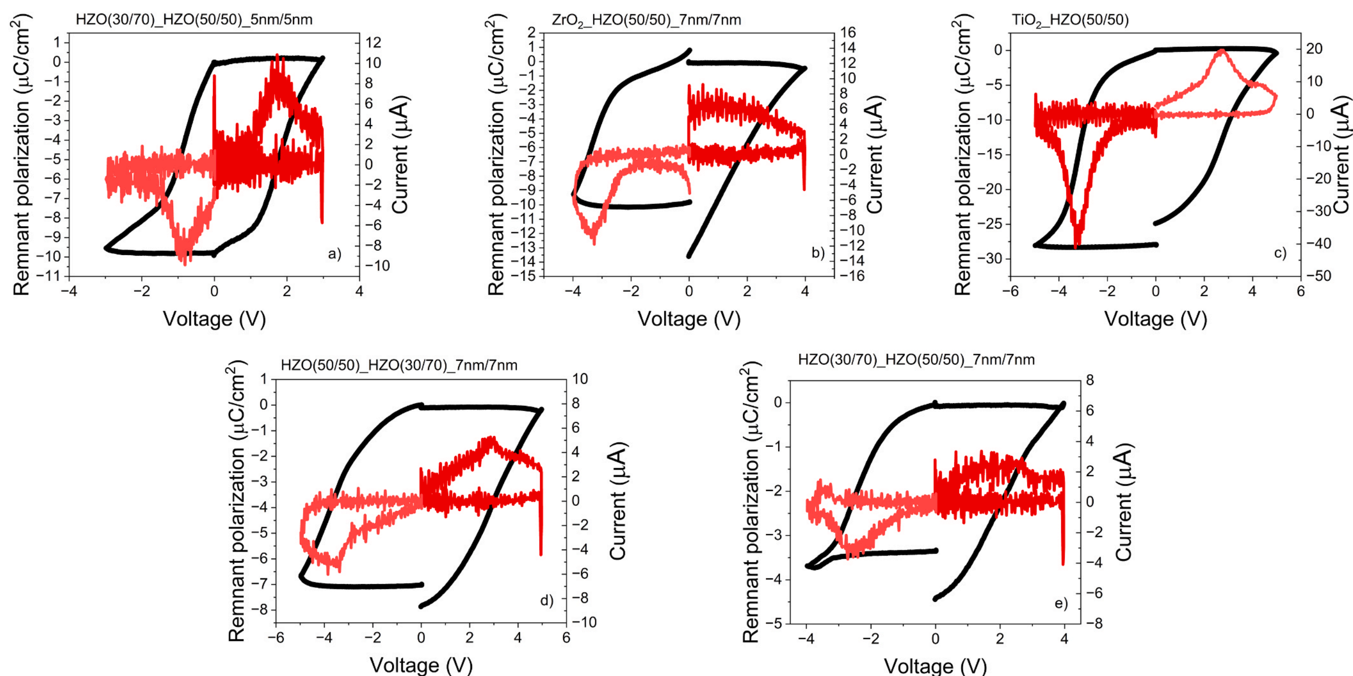

Fig. 8. The remnant polarization and current-voltage hysteresis cycles for multilayers structures of a) HZO(30/70)/HZO(50/50) with 5 nm/5 nm thickness of the layers; b) ZrO_2/HZO(50/50); c) TiO_2/HZO(50/50); d) HZO(50/50)/HZO(30/70) with 7 nm/7 nm thickness of the layers; e) HZO(30/70)/HZO(50/50) with 7 nm/ 7 nm thickness of the layers;.

reports on the dielectric constant for the orthorhombic phase of HZO. No other contribution or different value for series capacitance with non-ferroelectric contributions can explain the abnormal decrease in the dielectric constant for the 7 nm sample. However, these decreased values for this thickness are in very good agreement with the PV hysteresis loop presented in Figure S1 and with XRD data. No monoclinic phase is observed in the XRD for this sample, and the large remnant polarization could certainly indicate that the majority of the volume is well crystallized and exhibits ferroelectric behavior. Therefore, we also exclude other contributions to the decreased dielectric constant. Compared with thicker samples, the coercive field is much larger, and the hysteresis loop is more rectangular. Since the coercive field is proportional to the polarization and inversely proportional to the dielectric constant [61] (equation S6), the increased coercive field suggests a decrease in the dielectric constant. Moreover, if we consider the charge obtained from the second pulse of the PUND method (where there are no switching contributions, as shown in Figure S1c), the variation of charge with voltage (which is proportional to the capacitance) is significantly reduced for the thinner sample. Thus, the measured low dielectric constant is in good agreement with the increased coercivity and more rectangular shape of the PV loop. This decrease in the dielectric constant with thickness was previously observed in epitaxial ferroelectric perovskites: in the absence of structural defects and with a rectangular PV shape, the electric response to small AC signals is very low and close to the background dielectric constant which seems to be very low 10–15 [62].

The 14 nm HZO(50/50) layer appears to have the highest dielectric constant across the entire frequency range. This higher dielectric constant, compared to the antiferroelectric-like (AFE) HZO(30/70), is unusual, as AFE-like phases generally exhibit a larger dielectric constant compared with FE in many cases of perovskites and in many reports on fluorites [3,63–65]. The increased dielectric constant of the 14 nm HZO (50/50) layer could be due to a possible mixing of AFE and FE phases, which might also explain the step-like switching observed in the polarization-voltage (PV) characteristics [3,65].

For cases where multilayers of HZO(30/70)/HZO(50/50) with 5 nm/5 nm thickness or ZrO_2/HZO(50/50) with 7 nm/7 nm the dielectric constant shows significantly higher values Fig. 9b). Both cases exhibit larger values compared to the dielectric constant of a simple 14 nm HZO(30/70) layer, but a distinct amplification of the dielectric constant is particularly observed when the layer thickness is reduced. In this case, a noticeable difference in dielectric constant across the entire frequency range is also evident, depending on the applied polarity, due to the strong internal field observed in the hysteresis. The dielectric

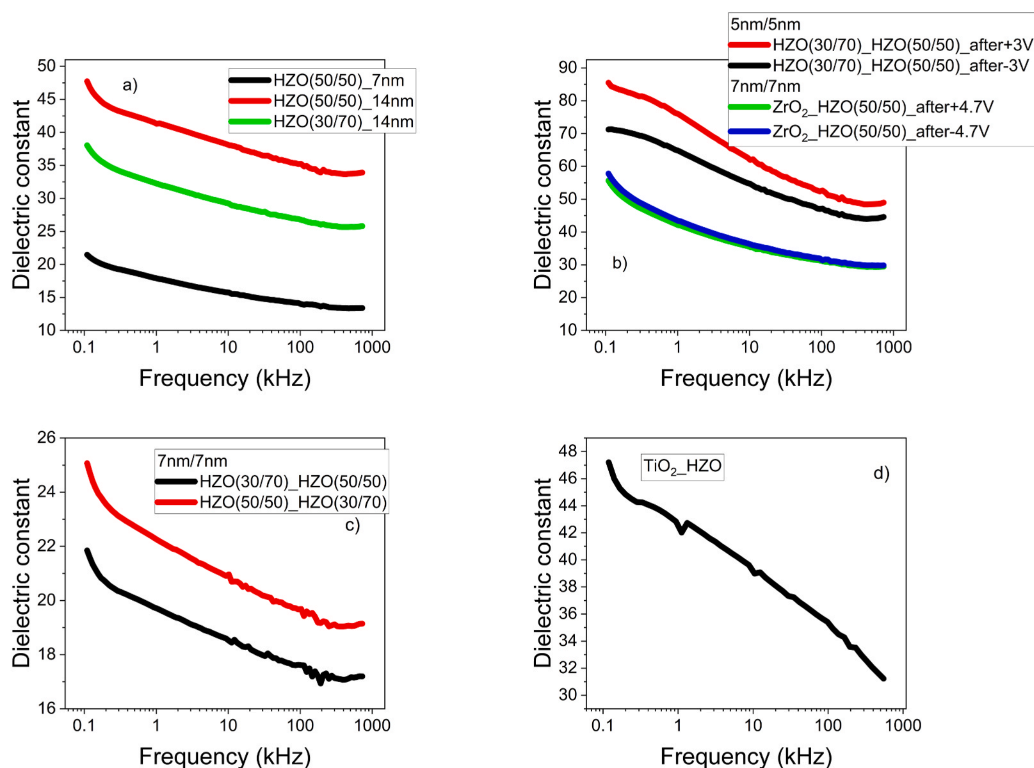

Fig. 9. The dielectric constant deduced from the measurements of capacitance and considering a correction from the influence of a $C_i = 6\mu C/cm^2$ for a)simple layers of HZO with different Hf/Zr ratio and different thickness b) for HZO(30/70)/HZO(50/50) with 5 nm/5 nm thickness measured after different polarization and for ZrO_2/HZO(50/50); c) HZO(30/70)/HZO(50/50) and HZO(50/50)/HZO(30/30) for 7 nm/7 nm; d) TiO_2/HZO(50/50);.

constant for the 14 nm multilayers combining HZO(50/50)_HZO(30/70) represented in Fig. 9c) shows a slightly higher value compared to the 7 nm HZO(50/50) layer but lower than that of HZO(30/70) or thicker HZO(50/50) layers (Fig. 9a)). The amplification of the dielectric constant compared to the constituent layers remains questionable in these cases. For the HZO-TiO_2 structure (Fig. 9d)), the dielectric constant remains similar in value and is very close to that of simple HZO(50/50) _14 nm.

Increased dielectric constant for the first two multilayered examples together with larger polarization compared with the last two examples of multilayers are associated with differences in structural characteristics as are evidenced in XRD. The first two multilayered samples have only orthorhombic/tetragonal components, while the last two have a significant amount of monoclinic phase. Considering the contribution of this non-Fe phase for HZO(30/70)-HZO(50/50) with 14 nm thickness, Eq. 2 becomes:

$$\varepsilon_1\varepsilon_0 E_1 + P_1 = \varepsilon_m\varepsilon_0 E_m = \varepsilon_2\varepsilon_0 E_2 + P_2 \tag{4}$$

$$V_{app} = V_1 + V_2 + V_m \tag{5}$$

where ε_m is the relative permittivity of the dielectric interlayer, and E_m is the electric field in the respective layer.

Such electrostatic considerations could explain the lack of polarization saturation and the wide distribution of coercive voltages, due to large internal fields that may arise, leading to a decrease in total charge and destabilization of polarization.

In an ideal case, considering the remnant polarization of HZO(50/50) around 20 $\mu C/cm^2$ and that of HZO(30/70) around 5 $\mu C/cm^2$, along with their dielectric constants at 100 kHz, an internal field equivalent of a voltage of approximately 4 V is obtained according to formula 3 for the 7 nm/7 nm configuration. This internal voltage is linked to the lack of polarization saturation in the two multilayer cases. With a significant amount of non-ferroelectric monoclinic phase, this field could be even higher, or much of the applied field could be distributed across the non-ferroelectric phase to compensate for polarization, as per formula 4 and 5. Considering that this internal field is higher that the coercive voltage for 7 nm or 14 nm HZO(50/50) and also opposite oriented to polarization in ferroelectric layer, it can be assumed that will determine the polarization instability since it acts as a depolarization field. This could also be related with low orthorhombic/tetragonal phase stabilization.

For the 5 nm/5 nm configuration, the internal voltage according to formula 3 is 2.8 V, very close to the coercive voltage of a simple 7 nm HZO(50/50) layer. Given that the induced internal field opposes the polarization direction in the layer with higher polarization, we can assume the HZO(50/50) layer is near coercivity and could stabilize a negative capacitance regime. Meanwhile, in the HZO(30/70) layer, the internal voltage aligns with the polarization direction, placing this layer in a ferroelectric state rather than an nonpolar state, as it is at zero bias. Thus, the antiferroelectric-like character disappears in the switching of the multilayer samples.

The dielectric constant of zirconium dioxide (ZrO_2) varies depending on factors such as crystalline phase, film thickness, and measurement frequency. Reported values range from approximately 20 to above 30 [66–68]. Thus for 7 nm we expect to have a 3.8 μF/cm [2]. The dielectric constant of titanium dioxide (TiO_2) varies depending on its crystalline phase and measurement conditions and is consider around 30–60 [69, 70] for low temperature processing. Thus for 6 nm the specific capacitance will be around 3.8–7.6 μF/cm [2]. These values are higher compared to the specific capacitance values measured for the multilayers that contain these material layers. Thus, stabilization of NC in these multilayers is excluded.

However, a clear enhancement is observed compared to simple layers, especially when considering the series connection between the capacitance of the dielectric and the FE layer (ranging between 1.3–0.9 $\mu F/cm^2$ for ZrO_2-HZO(50/50)). Additionally, using Eq. 3 and the values for specific capacitance of ZrO_2 and HZO (50/50) layers, an

internal field of about 2.6 V is expected, which is very similar to the internal field observed in the hysteresis loop. Therefore, in the case of multilayers, the presence of internal fields and the enhancement of capacitance can be well explained by the induced field resulting from different electrostatic conditions between the layers. In particular, for the HZO(30/70)_HZO(50/50) structure with 5 nm/5 nm layers, this internal field—induced by the polarization difference—is very close in magnitude to the coercive voltage of 7 nm HZO(50/50). As a result, the ferroelectric layer is driven into a polarization state associated with increased capacitance compared to the stable polarization states of a single-layer structure.

For the case of TiO_2/HZO(50/50), the equivalent series capacitance is between 1.1 and 1.6 μF/cm^2. The measured capacitance is higher compared to these series capacitance values, even though it does not exceed the capacitance of the simple thin film of HZO(50/50) with a similar thickness. Thus, in this case, we can hypothesize that electrostatic coupling could occur, but it would be less strong.

Besides the electrostatic considerations mentioned above, the shape of the dielectric constant/capacitance with frequency is essential in understanding the dielectric behavior of these materials and multilayer thin film structures. For example, on a semilogarithmic scale, simple layers exhibit a small linear decrease in capacitance with increasing frequency. This is usually associated with a delay in the response of the FE domains to the applied fields. However, polarization is known to respond much faster, and in this frequency range, contributions from non-FE components are expected to influence this behavior. In the previous analysis, we considered only the contribution of a series capacitance, but series elements could be formed from a very complex equivalent circuit with non-ideal elements. However, the small decrease in capacitance with frequency could also be associated with the contribution of other circuit elements, such as the resistivity of the substrate or electrodes, as well as the dielectric response of the grain boundaries in these polycrystalline thin films. When constructing multilayers, a Maxwell-Wagner relaxation [71] is typically expected, particularly due to the fact that not only the capacitance of the layers contributes to the overall capacitance but also the different resistivities of the layers. In our case, the multilayers seem to exhibit a similar behavior to simple thin films of HZO, with the exception of the 5 nm/5 nm and HZO(30/70)_HZO(50/50) multilayers. In the first case, a stepwise decrease in capacitance is indeed observed, even though the dielectric losses are very small and no peak is present. This could be associated with Maxwell-Wagner relaxation. This means that at higher frequencies, the capacitance is determined by the series combination of the capacitances of the two layers, whereas at lower frequencies, space charge accumulation could lead to such large increase in the deduced dielectric constant (at low frequencies). In the case of the TiO_2/HZO structure, a much larger decrease in capacitance with frequency is observed. Additionally, considering the hysteresis characteristics of this structure, we can hypothesize that the contribution of the TiO_2 layer does not behave as a simple series capacitor. If the TiO_2 layer acted purely as an insulator, an imprint field of at least 1.5 V should be observed (considering Eq. 3) as for ZrO_2/HZO. Moreover, no polarization decrease is detected compared to the simple HZO layer, as an exception compared with the other multilayers. On the contrary, the switching peaks are broader. Thus, we can conclude that the TiO_2 layer has a significant resistivity contribution [43]. During thermal annealing in a reduced oxygen atmosphere, oxygen vacancies are formed, leading to n-type doping, which influences the overall electrical response of the structure. Thus, the charges from TiO_2 could contribute to polarization compensation, and reduce the electrostatic coupling as for the other multilayers. A small decrease of capacitance with frequency has previously been reported in HZO-based thin films [72,73]. In [73], the decrease of capacitance with frequency is attributed to a parallel resistance of the ferroelectric layer related to different leakage conduction mechanisms, as well as to a frequency-dependent non-ideal parallel capacitance associated with interface traps at the metal/HZO interface. The study also considers the possible formation of sub-stoichiometric metallic oxides at the electrode interface, which can further influence the overall capacitance–frequency response.

Depending on the multilayer structure, constituent materials, and their thicknesses, different electrostatic conditions can be established, which influence both ferroelectric polarization switching and dielectric behavior. If strong internal fields are induced, they can lead to the destabilization of ferroelectricity and promote the stabilization of the monoclinic phase. When the internal electrostatic fields are close to the coercive field, the system may be stabilized in a ferroelectric state with increased capacitance.

Moreover, internal fields oriented opposite to the polarization direction are associated with a decrease in the total charge measured in polarization-voltage (P–V) loops. Such internal fields in multilayers are also linked to a shift of the P–V hysteresis along the voltage axis. These phenomena are observed in HZO(50/50)_HZO(30/70) and ZrO_2_HZO (50/50) multilayers. The large imprint observed in ZrO_2_HZO(50/50), compared to HZO(50/50)_HZO(30/70) multilayers, suggests that in FE/DE systems the internal fields are permanent, leading to the stabilization of only one polarization state. In contrast, in FE1/FE2 systems, the polarization appears to have two stable states.

In contrast, in the case of TiO_2/HZO(50/50), the higher polarization values, the absence of internal field effects, and the increased coercive voltages are associated with reduced internal field formation. This is likely due to the increased conductivity of the TiO_2 layer, which partially compensates the polarization at the ferroelectric/dielectric interface.

Depositing the TiN top electrode before the rapid thermal annealing (RTA) process can induce tensile stress on the hafnium zirconium oxide (HZO) film. This stress promotes the stabilization of the ferroelectric orthorhombic phase, thereby enhancing ferroelectric properties [74–76]. TiN electrodes can also influence the formation and distribution of oxygen vacancies within the ferroelectric layer [65,77–79]. These vacancies play a crucial role in the polarization wake-up effect, which is essential for achieving optimal ferroelectric performance.

Additional GIXRD results detailing the TiN-induced increase of the orthorhombic phase in 14 nm HZO(50/50), the reduction of the monoclinic component, and the stacking-sequence dependence observed in 7 nm/7 nm bilayers (including ZrO_2/HZO and 5 nm/5 nm cases) are provided in the Supplementary Information (5; Figures S5).

The influence of depositing a TiN top electrode prior to RTA on the electrical behavior of single HZO layers is detailed in the Supplementary Information (Section S6; Figure S6). Briefly, thicker HZO(50/50) and HZO(30/70) films show modest increases in polarization and permittivity—consistent with the reduced monoclinic fraction seen by XRD—whereas 7 nm HZO(50/50) displays a shift toward AFE-like P–V loops with higher remanent polarization and ~70 % higher capacitance. We attribute these trends to Ti oxidation and the resulting oxygen-vacancy gradient near the TiN/HZO interface, which is more impactful in thin films due to stronger depolarizing fields.

For bilayers of HZO(30/70)/HZO(50/50) with a total thickness of 14 nm, the influence of the TiN top electrode is presented in Fig. 10. Even though the remnant polarization remains unchanged (deduced from PUND), it can be observed that in this case, the hysteresis is saturated, and switching is clearly evidenced by a rectangular hysteresis loop. These structures with a TiN top electrode exhibit higher resistance to strong electric fields, and polarization saturation is evident. In these cases, the coercive voltages are closer to the 4 V internal voltage predicted by Eq. 3, as discussed in the previous section. These changes can be attributed to an increase in the orthorhombic phase, as observed in XRD measurements. However, the presence of a comparable amount of non-FE phases induces large depolarization fields, which could explain the lower polarization, beside internal fields. Additionally, the dielectric constant is significantly reduced to approximately 10. On the one hand, this reduction could be related to the rectangular shape of the P-V hysteresis loop, where dP/dV approaches zero for a stably switched polarization. This is also similar with the case of epitaxially thin films of

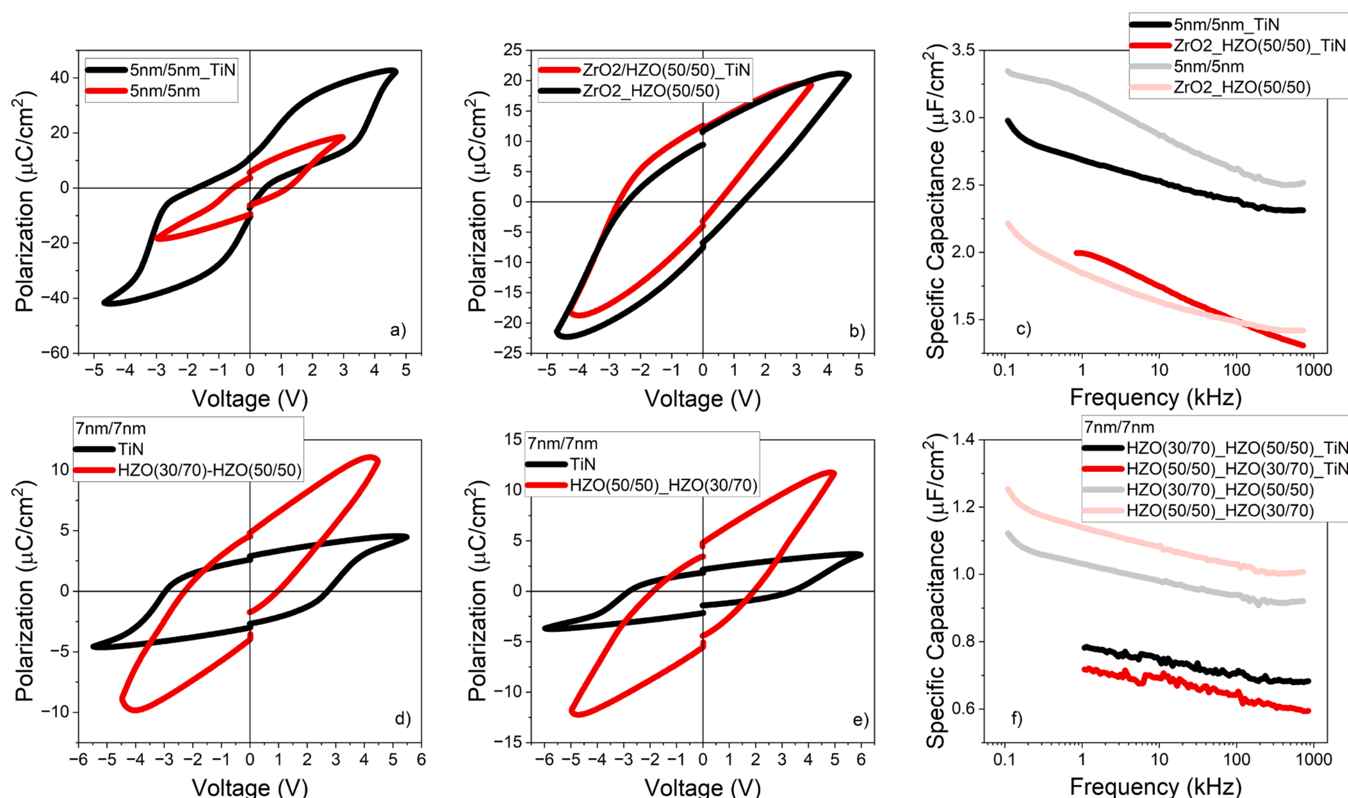

Fig. 10. The differences between characteristics of the multilayers annealed with or without TiN top electrode: a) HZO(30/70)/HZO(50/50) with 5 nm/5 nm thickness of the layers; b) ZrO_2/HZO(50/50); c) specific capacitance for 5 nm/5 nm and for ZrO2/HZO(50/50) d) HZO(50/50)/HZO(30/70) with 7 nm/7 nm thickness of the layers; e) HZO(30/70)/HZO(50/50) with 7 nm/7 nm thickness of the layers; f) specific capacitance for HZO(50/50)/HZO(30/70) and for HZO(30/70)/HZO(50/50) with 7 nm/7 nm thickness.

perovskites with rectangular PV and reduced dielectric constant [62,80,81]. On the other hand, the presence of a non-FE component in series could also contribute to the decrease in equivalent capacitance.

The effect of the TiN top electrode on the properties of HZO(30/70)_HZO(50/50) with a lower thickness, as well as on ZrO_2/HZO structures, is presented in Fig. 10. The case of HZO(30/70)_HZO(50/50) with a lower thickness is more complex. Even though XRD does not indicate a clear modification, the switching behavior is distinctly different. A clear AFE-like behavior is observed, with a very large saturated polarization in the FE phase exceeding 40 μC/cm². Considering a similar influence of oxygen vacancy formation as in thinner HZO50/50, it is reasonable to assume that in this thinner film, the tetragonal phase is more stable compared to the orthorhombic phase. This scenario is plausible since these two phases are difficult to distinguish using XRD. If an AFE-like phase is also induced in the bottom layer, the polarization difference is reduced, leading to a decrease in internal fields and, consequently, a reduction in the dielectric constant. As seen in Fig. 10c, the transition from FE to AFE-like behavior in this particular case is not accompanied by an increase in capacitance; on the contrary, it results in a decrease in capacitance. This contradicts previous reports suggesting that a mixture of AFE-like and FE or AFE-like behavior leads to an increase in the dielectric constant [36,65]. However, this result supports our assumption of electrostatic coupling between the constituent layers. As both layers transition toward AFE-like behavior, the polarization difference decreases, weakening the electrostatic coupling. This provides further evidence that electrostatic interactions in HZO multilayers can be influenced by phase instabilities and defect formation.

The introduction of a TiN top electrode prior to rapid thermal annealing significantly influences the phase composition, electrical behavior, and electrostatic interactions within HZO-based simple and multilayer structures. These effects are mediated through stress-induced stabilization of the orthorhombic phase and the generation of oxygen vacancies, which are particularly impactful in thinner films. While TiN generally enhances ferroelectric properties by promoting orthorhombic phase formation and increasing polarization, it can also induce AFE-like behavior and modify the dielectric response. The observed variations between simple and multilayer structures with and without TiN electrode, emphasize the critical role of electrode in determining the functional properties of HZO-based devices. Even though in simple layers the TiN top electrode appears to enhance both ferroelectric and dielectric properties, in multilayers it seems to have a detrimental effect. In thinner structures, it induces an AFE-like behavior, which leads to weaker electrostatic coupling between layers and a consequent decrease in capacitance. In thicker multilayers, although the monoclinic phase is reduced and the orthorhombic/tetragonal phase content increases, the P-V characteristics show no improvement in polarization values, exhibit larger coercive voltages, and display a reduced capacitance.

5. Conclusions

In this study, we provide a comprehensive analysis of how polarization switching and the dielectric constant are influenced by electrostatic considerations in multilayers based on ferroelectric HZO. Our study is extensive, covering a wide range of samples and configurations to systematically evaluate the interplay between electrostatic effects, structural changes, and defect formation in HZO-based multilayers.

Given that HZO can readily transition between different structural phases and is prone to oxygen vacancy formation, we carefully assessed the impact of layer thickness, Hf/Zr ratio, and the presence of a TiN top electrode. By constructing multilayers with alternating HZO compositions and HZO/DE structures, we aimed to distinguish between effects driven by electrostatics, those arising from structural phase changes, and

those influenced by oxygen vacancies.

The experimental data provide clear evidence of electrostatic coupling in specific HZO-based multilayer structures, notably HZO(30/70)/HZO(50/50) (5 nm/5 nm) and ZrO_2/HZO(50/50) (7 nm/7 nm), where a significant enhancement of the effective dielectric constant is observed compared to single layers: 70–80 measured at 1 kHz for HZO (30/70)/HZO(50/50) (5 nm/5 nm) and 45 for ZrO_2/HZO(50/50) (7 nm/7 nm). This enhancement is attributed to internal electric fields generated by polarization mismatch between adjacent layers, with estimated internal voltages of approximately 2.8 V and 2.6 V, respectively—values comparable to the coercive voltage of thinner HZO(50/50) films. Such internal fields can drive the ferroelectric layer into a near-coercive regime, potentially stabilizing a negative capacitance response. In contrast, multilayers such as HZO(50/50)/HZO(30/70) (7 nm/7 nm) and HZO(30/70)/HZO(50/50) (14 nm/14 nm), which could have a theoretical 4 V internal voltage exceeding the coercive voltage, exhibit significant monoclinic phase content, show only modest or no capacitance enhancement, and are consistent with reduced ferroelectric stability. The TiO_2/HZO(50/50) structure also does not show substantial capacitance amplification, likely due to the resistive behavior of TiO_2 and the presence of compensating charges that weaken electrostatic coupling. The target is to use electrostatic couplings to induce enhancement of the dielectric constant compared with simple layers, aiming to improve the performance of ferroelectric materials for advanced applications in electronic devices, particularly for those requiring high capacitance and stability under varying conditions. However, electrostatic couplings are also shown to exist in samples that only exhibit an increase in capacitance compared with the equivalent series resistance of the constituent layers.

This comprehensive evaluation provides deeper insight into optimizing the dielectric properties and switching behavior of HZO-based thin films for potential applications in negative capacitance devices and advanced electronic components. Future work should focus on refining processing conditions to further control phase composition and enhance ferroelectric stability in these systems.

Associated content

Supporting Information. Additional theoretical details analysis, supplemental electrical characterizations can be found in Supporting Information file. The following files are available free of charge. Supporting Information (file type, i.e., PDF).

Author information

Author's contribution

A.G.B. conceived the study, performed the electrical characterization, and wrote the first draft of the manuscript. P.T. prepared the samples. D.P. performed and analyzed XRD data. C.R. performed and analyzed the TEM measurements. S.L. performed the photolithography of the top electrodes. L.P. and A.D. supervised the project, secured funding, and revised the manuscript. All authors discussed the results and contributed to the final version of the manuscript.

CRediT authorship contribution statement

ATHANASIOS DIMOULAS: Writing – review & editing, Funding acquisition. **CRISTIAN RADU:** Methodology. **LUCIAN PINTILIE:** Writing – review & editing, Funding acquisition. **SARA LAAFAR:** Methodology. **Boni Andra-Georgia:** Writing – original draft, Methodology, Investigation, Conceptualization. **DANA POPESCU:** Writing – review & editing, Methodology. **POLYCHRONIS TSIPAS:** Writing – review & editing, Methodology.

Funding

PNRR project 760239/28.12.2023, funded by the Romanian Ministry of Research, Innovation and Digitization through the National Recovery and Resilience Plan and Core Program, component project PN23080303, funded by Romanian Ministry of Research, Innovation and Digitization.

Declaration of Competing Interest

The authors declare the following financial interests/personal relationships which may be considered as potential competing interests: Andra Georgia Boni reports financial support was provided by National Institute of Materials Physics. Andra Georgia Boni reports a relationship with National Institute of Materials Physics that includes: employment. If there are other authors, they declare that they have no known competing financial interests or personal relationships that could have appeared to influence the work reported in this paper.

Acknowledgments

The authors acknowledge financial support through the PNRR project 760239/28.12.2023, funded by the Romanian Ministry of Research, Innovation and Digitization through the National Recovery and Resilience Plan. D.P and C.R authors acknowledge financial support through the Core Program, component project PN23080303, funded by Romanian Ministry of Research, Innovation and Digitization.

Appendix A. Supporting information

Supplementary data associated with this article can be found in the online version at doi:10.1016/j.jallcom.2025.184617.

References

[1] T.S. Böscke, J. Müller, D. Bräuhaus, U. Schröder, U. Böttger, Ferroelectricity in hafnium oxide thin films, Appl. Phys. Lett. 99 (10) (2011) 102903, https://doi.org/10.1063/1.3634052.

[2] J.Y. Park, D.H. Lee, K. Yang, S.H. Kim, G.T. Yu, G.H. Park, E.B. Lee, K.H. Kim, M. H. Park, Engineering strategies in emerging fluorite-structured ferroelectrics, ACS Appl. Electron. Mater. 4 (4) (2022) 1369–1380, https://doi.org/10.1021/acsaelm.1c00792.

[3] A. Kashir, M.G. Farahani, H. Hwang, Towards an ideal high-κ HfO2–ZrO2-based dielectric, Nanoscale 13 (32) (2021) 13631–13640, https://doi.org/10.1039/D1NR02272E.

[4] K. Ni, A. Saha, W. Chakraborty, H. Ye, B. Grisafe, J. Smith, G.B. Rayner, S. Gupta, S. Datta, Equivalent oxide thickness (EOT) scaling with hafnium zirconium oxide high-κ dielectric near morphotropic phase boundary, 2019 IEEE Int. Electron Devices Meet. (2019) 7.4.1–7.4.4, https://doi.org/10.1109/IEDM19573.2019.8993495.

[5] M. Jung, V. Gaddam, S. Jeon, A review on morphotropic phase boundary in fluorite-structure hafnia towards DRAM technology, Nano Converg. 9 (1) (2022) 44, https://doi.org/10.1186/s40580-022-00333-7.

[6] H. Chen, X. Zhou, L. Tang, Y. Chen, H. Luo, X. Yuan, C.R. Bowen, D. Zhang, HfO2-based ferroelectrics: from enhancing performance, material design, to applications, Appl. Phys. Rev. 9 (1) (2022) 011307, https://doi.org/10.1063/5.0066607.

[7] M.H. Park, Y.H. Lee, H.J. Kim, Y.J. Kim, T. Moon, K.D. Kim, J. Müller, A. Kersch, U. Schroeder, T. Mikolajick, C.S. Hwang, Ferroelectricity and antiferroelectricity of doped thin HfO2-based films, Adv. Mater. 27 (11) (2015) 1811–1831, https://doi.org/10.1002/adma.201404531.

[8] R. Materlik, C. Künneth, A. Kersch, The origin of ferroelectricity in Hf1−xZrxO2: a computational investigation and a surface energy model, J. Appl. Phys. 117 (13) (2015) 134109, https://doi.org/10.1063/1.4916707.

[9] C. Richter, T. Schenk, M.H. Park, F.A. Tscharntke, E.D. Grimley, J.M. LeBeau, C. Zhou, C.M. Fancher, J.L. Jones, T. Mikolajick, U. Schroeder, Si doped hafnium oxide—A "Fragile" ferroelectric system, Adv. Electron. Mater. 3 (10) (2017) 1700131, https://doi.org/10.1002/aelm.201700131.

[10] K. Chae, J. Hwang, E. Chagarov, A. Kummel, K. Cho, Stability of ferroelectric and antiferroelectric hafnium–zirconium oxide thin films, J. Appl. Phys. 128 (5) (2020) 054101, https://doi.org/10.1063/5.0011547.

[11] W. Liu, Z. Weng, J. Li, W. Yan, Y. Qu, Y. Zhao, Orthorhombic-I (Pbca) phase: origin of anti-ferroelectricity in HfZrO films, 2024 IEEE 17th Int. Conf. SolidState Integr. Circuit Technol. (2024) 1–3, https://doi.org/10.1109/ICSICT62049.2024.10832105.

[12] S. Oh, H. Jang, H. Hwang, Composition optimization of HfxZr1-xO2 thin films to achieve the morphotrophic phase boundary for high-k dielectrics, J. Appl. Phys. 133 (15) (2023) 154102, https://doi.org/10.1063/5.0127171.

[13] M.H. Park, Y.H. Lee, H.J. Kim, Y.J. Kim, T. Moon, K.D. Kim, S.D. Hyun, C. S. Hwang, Morphotropic phase boundary of Hf1−xZrxO2 thin films for dynamic random access memories, ACS Appl. Mater. Interfaces 10 (49) (2018) 42666–42673, https://doi.org/10.1021/acsami.8b15576.

[14] M. Lee, Y.C. Jung, J.-H. Kim, D.M. Narayan, S. Kang, W.Y. Park, K. Im, J. Kim, Effect of La and Si additives in Zr-doped HfO2 capacitors for pseudo-linear high-κ dielectric applications, Nano Converg. 12 (1) (2025) 15, https://doi.org/10.1186/s40580-025-00477-2.

[15] X. Liu, W. Zhao, J. Wang, L. Yao, M. Ding, Y. Cheng, Enhancing the ferroelectric performance of Hf0.5Zr0.5O2 films by optimizing the incorporation of Al dopant, Nanotechnology 36 (13) (2025), https://doi.org/10.1088/1361-6528/adaf2c.

[16] M. Ghiasabadi Farahani, A. Quintana, T. Song, R. Kumar, A. Rubano, F. Ali, F. Sánchez, I. Fina, Dual ferroelectric polarization and dielectric response improvement in epitaxial Hf0.5Zr0.5O2/HfO2 nanolaminates, ACS Appl. Mater. Interfaces 17 (2) (2025) 3570–3577, https://doi.org/10.1021/acsami.4c15867.

[17] H.J. Zhao, Y. Fu, L. Yu, Y. Wang, Y. Yang, L. Bellaiche, Y. Ma, Creating ferroelectricity in monoclinic $({\mathrm{HfO}}_{2}{})_{1}/({\mathrm{CeO}}_{2}{})_{1}$ superlattices, Phys. Rev. Lett. 132 (25) (2024) 256801, https://doi.org/10.1103/PhysRevLett.132.256801.

[18] M.H. Park, H.J. Kim, G. Lee, J. Park, Y.H. Lee, Y.J. Kim, T. Moon, K.D. Kim, S. D. Hyun, H.W. Park, H.J. Chang, J.-H. Choi, C.S. Hwang, A comprehensive study on the mechanism of ferroelectric phase formation in hafnia-zirconia nanolaminates and superlattices, Appl. Phys. Rev. 6 (4) (2019) 041403, https://doi.org/10.1063/1.5118737.

[19] M. Kang, Y. Peng, W. Xiao, Y. Zhang, Z. Wang, P. Du, H. Jiang, F. Liu, Y. Liu, Y. Hao, G. Han, HfO2–ZrO2 ferroelectric capacitors with superlattice structure: improving fatigue stability, fatigue recovery, and switching speed, ACS Appl. Mater. Interfaces 16 (2) (2024) 2954–2963, https://doi.org/10.1021/acsami.3c15732.

[20] S. Oh, H. Jang, H. Hwang, Accurate evaluation of high-k HZO/ZrO2 films by morphotropic phase boundary, IEEE Electron Device Lett. 45 (1) (2024) 28–31, https://doi.org/10.1109/LED.2023.3331001.

[21] N. Bai, K.-H. Xue, J. Huang, J.-H. Yuan, W. Wang, G.-Q. Mao, L. Zou, S. Yang, H. Lu, H. Sun, X. Miao, Designing wake-up free ferroelectric capacitors based on the HfO2/ZrO2 superlattice structure, Adv. Electron. Mater. 9 (1) (2023) 2200737, https://doi.org/10.1002/aelm.202200737.

[22] Y. Yun, L. Mühlenbein, D.S. Knoche, A. Lotnyk, A. Bhatnagar, Strongly enhanced and tunable photovoltaic effect in ferroelectric-paraelectric superlattices, Sci. Adv. 7 (23) (2021) eabe4206, https://doi.org/10.1126/sciadv.abe4206.

[23] P. Zubko, N. Jecklin, A. Torres-Pardo, P. Aguado-Puente, A. Gloter, C. Lichtensteiger, J. Junquera, O. Stéphan, J.-M. Triscone, Electrostatic coupling and local structural distortions at interfaces in ferroelectric/paraelectric superlattices, Nano Lett. 12 (6) (2012) 2846–2851, https://doi.org/10.1021/nl3003717.

[24] J.L. Lin, Y. Sun, R. He, Y. Li, Z. Zhong, P. Gao, X. Zhao, Z. Zhang, Z.J. Wang, Colossal room-temperature ferroelectric polarizations in SrTiO3/SrRuO3 superlattices induced by oxygen vacancies, Nano Lett. 22 (17) (2022) 7104–7111, https://doi.org/10.1021/acs.nanolett.2c02175.

[25] S.S. Cheema, N. Shanker, L.-C. Wang, C.-H. Hsu, S.-L. Hsu, Y.-H. Liao, M. San Jose, J. Gomez, W. Chakraborty, W. Li, J.-H. Bae, S.K. Volkman, D. Kwon, Y. Rho, G. Pinelli, R. Rastogi, D. Pipitone, C. Stull, M. Cook, B. Tyrrell, V.A. Stoica, Z. Zhang, J.W. Freeland, C.J. Tassone, A. Mehta, G. Saheli, D. Thompson, D.I. Suh, W.-T. Koo, K.-J. Nam, D.J. Jung, W.-B. Song, C.-H. Lin, S. Nam, J. Heo, N. Parihar, C.P. Grigoropoulos, P. Shafer, P. Fay, R. Ramesh, S. Mahapatra, J. Ciston, S. Datta, M. Mohamed, C. Hu, S. Salahuddin, Ultrathin ferroic HfO2–ZrO2 superlattice gate stack for advanced transistors, Nature 604 (7904) (2022) 65–71, https://doi.org/10.1038/s41586-022-04425-6.

[26] A. Kashir, H. Hwang, A CMOS-compatible morphotropic phase boundary, Nanotechnology 32 (44) (2021) 445706, https://doi.org/10.1088/1361-6528/ac1716.

[27] M. Jung, V. Gaddam, S. Jeon, A review on morphotropic phase boundary in fluorite-structure hafnia towards DRAM technology, Nano Converg. 9 (1) (2022) 44, https://doi.org/10.1186/s40580-022-00333-7.

[28] X. Du, H. Zhu, S. Shen, Y. Yin, X. Li, Enhancement of both dielectric and ferroelectric performances in TiN/Al2O3/Hf1-xZrxO2/TiO2/TiN -based 3D capacitors, Trans. Mater. Res. 1 (4) (2025) 100068, https://doi.org/10.1016/j.tramat.2025.100068.

[29] Ni, K.; Datta, S.; Kummel, A. Non-Volatile Multi-Level Cell Memory Using a Ferroelectric Superlattice and Related Systems. US11532355B2, December 20, 2022. ⟨https://patents.google.com/patent/US11532355B2/en⟩ (accessed 2025-03-28).

[30] R. Wang, H. Ye, X. Xu, J. Wang, R. Feng, T. Wang, B. Sheng, F. Liu, B. Shen, P. Wang, X. Wang, Composition-graded nitride ferroelectrics based multi-level non-volatile memory for neuromorphic computing, Adv. Mater. 37 (5) (2025) 2414805, https://doi.org/10.1002/adma.202414805.

[31] G. A. Boni, L. D. Filip, C. Chirila, I. Pasuk, R. Negrea, I. Pintilie, L. Pintilie, Multiple polarization states in symmetric ferroelectric heterostructures for multi-bit non-volatile memories, Nanoscale 9 (48) (2017) 19271–19278, https://doi.org/10.1039/C7NR06354G.

[32] A.G. Boni, C. Chirila, I. Pasuk, R. Negrea, I. Pintilie, L. Pintilie, Steplike switching in symmetric PbZr0.2Ti0.8O3/CoFeO4/PbZr0.2Ti0.8O3 heterostructures for multistate ferroelectric memory, Phys. Rev. Appl. 8 (2017), https://doi.org/10.1103/PhysRevApplied.8.034035.

[33] K.D. Kim, Y.J. Kim, M.H. Park, H.W. Park, Y.J. Kwon, Y.B. Lee, H.J. Kim, T. Moon, Y.H. Lee, S.D. Hyun, B.S. Kim, C.S. Hwang, Transient negative capacitance effect in atomic-layer-deposited Al2O3/Hf0.3Zr0.7O2 bilayer thin film, Adv. Funct. Mater. 29 (17) (2019) 1808228, https://doi.org/10.1002/adfm.201808228.

[34] M. Hoffmann, F.P.G. Fengler, M. Herzig, T. Mittmann, B. Max, U. Schroeder, R. Negrea, P. Lucian, S. Slesazeck, T. Mikolajick, Unveiling the double-well energy landscape in a ferroelectric layer, Nature 565 (7740) (2019) 464–467, https://doi.org/10.1038/s41586-018-0854-z.

[35] M. Hoffmann, F.P.G. Fengler, B. Max, U. Schroeder, S. Slesazeck, T. Mikolajick, Negative capacitance for electrostatic supercapacitors, Adv. Energy Mater. 9 (40) (2019) 1901154, https://doi.org/10.1002/aenm.201901154.

[36] S.S. Cheema, N. Shanker, S.-L. Hsu, J. Schaadt, N.M. Ellis, M. Cook, R. Rastogi, R.C. N. Pilawa-Podgurski, J. Ciston, M. Mohamed, S. Salahuddin, Giant energy storage and power density negative capacitance superlattices, Nature 629 (8013) (2024) 803–809, https://doi.org/10.1038/s41586-024-07365-5.

[37] J.P.B. Silva, K.C. Sekhar, H. Pan, J.L. MacManus-Driscoll, M. Pereira, Advances in dielectric thin films for energy storage applications, revealing the promise of group IV binary oxides, ACS Energy Lett. 6 (6) (2021) 2208–2217, https://doi.org/10.1021/acsenergylett.1c00313.

[38] D.J.R. Appleby, N.K. Ponon, K.S.K. Kwa, B. Zou, P.K. Petrov, T. Wang, N.M. Alford, A. O'Neill, Experimental observation of negative capacitance in ferroelectrics at room temperature, Nano Lett. 14 (7) (2014) 3864–3868, https://doi.org/10.1021/nl5017255.

[39] W. Gao, A. Khan, X. Marti, C. Nelson, C. Serrao, J. Ravichandran, R. Ramesh, S. Salahuddin, Room-temperature negative capacitance in a ferroelectric–dielectric superlattice heterostructure, Nano Lett. 14 (10) (2014) 5814–5819, https://doi.org/10.1021/nl502691u.

[40] Experimental Observation of Negative Capacitance in Ferroelectrics at Room Temperature | Nano Letters. ⟨https://pubs.acs.org/doi/full/10.1021/nl5017255⟩ (accessed 2023-11-13).

[41] Y.J. Kim, H. Yamada, T. Moon, Y.J. Kwon, C.H. An, H.J. Kim, K.D. Kim, Y.H. Lee, S. D. Hyun, M.H. Park, C.S. Hwang, Time-dependent negative capacitance effects in Al2O3/BaTiO3 bilayers, Nano Lett. 16 (7) (2016) 4375–4381, https://doi.org/10.1021/acs.nanolett.6b01480.

[42] Y.J. Kim, M.H. Park, Y.H. Lee, H.J. Kim, W. Jeon, T. Moon, K. Do Kim, D.S. Jeong, H. Yamada, C.S. Hwang, Frustration of negative capacitance in Al2O3/BaTiO3 bilayer structure, Sci. Rep. 6 (1) (2016) 19039, https://doi.org/10.1038/srep19039.

[43] A.G. Boni, R. Patru, L.D. Filip, C. Chirila, I. Pasuk, I. Pintilie, L. Pintilie, Negative capacitance and switching dynamics control via non-ferroelectric elements, ACS Appl. Energy Mater. 5 (3) (2022) 3307–3318, https://doi.org/10.1021/acsaem.1c03890.

[44] H.W. Park, S.D. Hyun, I.S. Lee, S.H. Lee, Y.B. Lee, M. Oh, B.Y. Kim, S.G. Ryoo, C. S. Hwang, Polarizing and depolarizing charge injection through a thin dielectric layer in a ferroelectric–dielectric bilayer, Nanoscale 13 (4) (2021) 2556–2572, https://doi.org/10.1039/D0NR07597C.

[45] E. Yurchuk, J. Müller, S. Müller, J. Paul, M. Pešić, R. van Bentum, U. Schroeder, T. Mikolajick, Charge-trapping phenomena in HfO2-based FeFET-type nonvolatile memories, IEEE Trans. Electron Devices 63 (9) (2016) 3501–3507, https://doi.org/10.1109/TED.2016.2588439.

[46] A.Q. Jiang, H.J. Lee, G.H. Kim, C.S. Hwang, The inlaid Al2O3 tunnel switch for ultrathin ferroelectric films, Adv. Mater. 21 (28) (2009) 2870–2875, https://doi.org/10.1002/adma.200802924.

[47] Y.J. Kim, M.H. Park, W. Jeon, H.J. Kim, T. Moon, Y.H. Lee, K.D. Kim, S.D. Hyun, C. S. Hwang, Interfacial charge-induced polarization switching in Al2O3/Pb(Zr,Ti)O3 bi-layer, J. Appl. Phys. 118 (22) (2015) 224105, https://doi.org/10.1063/1.4937544.

[48] P. Zubko, J.C. Wojdeł, M. Hadjimichael, S. Fernandez-Pena, A. Sené, I. Luk'yanchuk, J.-M. Triscone, J. Íñiguez, Negative capacitance in multidomain ferroelectric superlattices, Nature 534 (7608) (2016) 524–528, https://doi.org/10.1038/nature17659.

[49] N. Siannas, C. Zacharaki, P. Tsipas, S. Chaitoglou, L. Bégon-Lours, C. Istrate, L. Pintilie, A. Dimoulas, Metastable ferroelectricity driven by depolarization fields in ultrathin Hf0.5Zr0.5O2, Commun. Phys. 5 (1) (2022) 1–10, https://doi.org/10.1038/s42005-022-00951-x.

[50] S.S. Cheema, D. Kwon, N. Shanker, R. dos Reis, S.-L. Hsu, J. Xiao, H. Zhang, R. Wagner, A. Datar, M.R. McCarter, C.R. Serrao, A.K. Yadav, G. Karbasian, C.-H. Hsu, A.J. Tan, L.-C. Wang, V. Thakare, X. Zhang, A. Mehta, E. Karapetrova, R. V. Chopdekar, P. Shafer, E. Arenholz, C. Hu, R. Proksch, R. Ramesh, J. Ciston, S. Salahuddin, Enhanced ferroelectricity in ultrathin films grown directly on silicon, Nature 580 (7804) (2020) 478–482, https://doi.org/10.1038/s41586-020-2208-x.

[51] E.D. Grimley, T. Schenk, X. Sang, M. Pešić, U. Schroeder, T. Mikolajick, J. M. LeBeau, Structural changes underlying field-cycling phenomena in ferroelectric HfO2 thin films, Adv. Electron. Mater. 2 (9) (2016) 1600173, https://doi.org/10.1002/aelm.201600173.

[52] C. Künneth, R. Materlik, A. Kersch, Modeling ferroelectric film properties and size effects from tetragonal interlayer in Hf1−xZrxO2 grains, J. Appl. Phys. 121 (20) (2017) 205304, https://doi.org/10.1063/1.4983811.

[53] Y. Cheng, Z. Gao, K.H. Ye, H.W. Park, Y. Zheng, Y. Zheng, J. Gao, M.H. Park, J.-H. Choi, K.-H. Xue, C.S. Hwang, H. Lyu, Reversible transition between the polar and antipolar phases and its implications for wake-up and fatigue in HfO2-based ferroelectric thin film, Nat. Commun. 13 (1) (2022) 645, https://doi.org/10.1038/s41467-022-28236-5.

[54] S. Mueller, J. Mueller, A. Singh, S. Riedel, J. Sundqvist, U. Schroeder, T. Mikolajick, Incipient ferroelectricity in Al-doped HfO2 thin films, Adv. Funct. Mater. 22 (11) (2012) 2412–2417, https://doi.org/10.1002/adfm.201103119.

[55] J. Müller, T.S. Böscke, U. Schröder, S. Mueller, D. Bräuhaus, U. Böttger, L. Frey, T. Mikolajick, Ferroelectricity in simple binary ZrO2 and HfO2, Nano Lett. 12 (8) (2012) 4318–4323, https://doi.org/10.1021/nl302049k.

[56] T. Shiraishi, K. Katayama, T. Yokouchi, T. Shimizu, T. Oikawa, O. Sakata, H. Uchida, Y. Imai, T. Kiguchi, T.J. Konno, H. Funakubo, Impact of mechanical stress on ferroelectricity in (Hf0.5Zr0.5)O2 thin films, Appl. Phys. Lett. 108 (26) (2016) 262904, https://doi.org/10.1063/1.4954942.

[57] S. Zhou, J. Zhang, A.M. Rappe, Strain-induced antipolar phase in hafnia stabilizes robust thin-film ferroelectricity, Sci. Adv. 8 (47) (2022) eadd5953, https://doi.org/10.1126/sciadv.add5953.

[58] S.T. Jaszewski, E.R. Hoglund, A. Costine, M.H. Weber, S.S. Fields, M.G. Sales, J. Vaidya, L. Bellcase, K. Loughlin, A. Salanova, D.A. Dickie, S.L. Wolfley, M. D. Henry, J.-P. Maria, J.L. Jones, N. Shukla, S.J. McDonnell, P. Reinke, P. E. Hopkins, J.M. Howe, J.F. Ihlefeld, Impact of oxygen content on phase constitution and ferroelectric behavior of hafnium oxide thin films deposited by reactive high-power impulse magnetron sputtering, Acta Mater. 239 (2022) 118220, https://doi.org/10.1016/j.actamat.2022.118220.

[59] J.F. Ihlefeld, S.T. Jaszewski, S.S. Fields, A perspective on ferroelectricity in hafnium oxide: mechanisms and considerations regarding its stability and performance, Appl. Phys. Lett. 121 (24) (2022) 240502, https://doi.org/10.1063/5.0129546.

[60] S.T. Jaszewski, S. Calderon, B. Shrestha, S.S. Fields, A. Samanta, F.J. Vega, J. D. Minyard, J.A. Casamento, J.-P. Maria, N.J. Podraza, E.C. Dickey, A.M. Rappe, T. E. Beechem, J.F. Ihlefeld, Infrared signatures for phase identification in hafnium oxide thin films, ACS Nano 17 (23) (2023) 23944–23954, https://doi.org/10.1021/acsnano.3c08371.

[61] Tagantsev, A.K.; Cross, L.E.; Fousek, J. Domains in Ferroic Crystals and Thin Films; Springer: New York, NY, 2010. https://doi.org/10.1007/978-1-4419-1417-0.

[62] G.A. Boni, C.F. Chirila, L. Hrib, R. Negrea, L.D. Filip, I. Pintilie, L. Pintilie, Low value for the static background dielectric constant in epitaxial PZT thin films, Sci. Rep. 9 (2019), https://doi.org/10.1038/s41598-019-51312-8.

[63] X. Wang, T. Yang, J. Shen, Y. Dong, Y. Liu, Phase transition and dielectric properties of (Pb,La)(Zr,Sn,Ti)O3 ceramics at morphotropic phase boundary, J. Alloy. Compd. 673 (2016) 67–72, https://doi.org/10.1016/j.jallcom.2016.02.217.

[64] V. Gaddam, G. Kim, T. Kim, M. Jung, C. Kim, S. Jeon, Novel approach to high κ (~59) and low EOT (~3.8 Å) near the morphotrophic phase boundary with AFE/FE (ZrO2/HZO) bilayer heterostructures and high-pressure annealing, ACS Appl. Mater. Interfaces 14 (38) (2022) 43463–43473, https://doi.org/10.1021/acsami.2c08691.

[65] Z. Zhao, Y.-R. Chen, J.-F. Wang, Y.-W. Chen, J.-R. Zou, Y. Lin, Y. Xing, C.W. Liu, C. Hu, Engineering Hf0.5Zr0.5O2 ferroelectric/anti- ferroelectric phases with oxygen vacancy and interface energy achieving high remanent polarization and dielectric constants, IEEE Electron Device Lett. 43 (4) (2022) 553–556, https://doi.org/10.1109/LED.2022.3149309.

[66] J.C. Garcia, L.M.R. Scolfaro, A.T. Lino, V.N. Freire, G.A. Farias, C.C. Silva, H.W. L. Alves, S.C.P. Rodrigues, E.F., Jr da Silva, Structural, electronic, and optical properties of ZrO2 from Ab initio calculations, J. Appl. Phys. 100 (10) (2006) 104103, https://doi.org/10.1063/1.2386967.

[67] J. Jeong, Y. Han, H. Sohn, Effect of La doping on dielectric constant and tetragonality of ZrO2 thin films deposited by atomic layer deposition, J. Alloy. Compd. 927 (2022) 166961, https://doi.org/10.1016/j.jallcom.2022.166961.

[68] J. Liu, J. Li, J. Wu, J. Sun, Structure and dielectric property of high-k ZrO2 films grown by atomic layer deposition using tetrakis(Dimethylamido)zirconium and ozone, Nanoscale Res. Lett. 14 (1) (2019) 154, https://doi.org/10.1186/s11671-019-2989-8.

[69] V. Bessergenev, High-temperature anomalies of dielectric constant in TiO2 thin films, Mater. Res. Bull. 44 (8) (2009) 1722–1728, https://doi.org/10.1016/j.materresbull.2009.03.014.

[70] A. Wypych, I. Bobowska, M. Tracz, A. Opasinska, S. Kadlubowski, A. Krzywania-Kaliszewska, J. Grobelny, P. Wojciechowski, Dielectric properties and characterisation of titanium dioxide obtained by different chemistry methods, J. Nanomater. 2014 (1) (2014) 124814, https://doi.org/10.1155/2014/124814.

[71] K.C. Kao, 2 - Electric Polarization and Relaxation, in: K.C. Kao (Ed.), In Dielectric Phenomena in Solids, Academic Press, San Diego, 2004, pp. 41–114, https://doi.org/10.1016/B978-012396561-5/50012-8.

[72] M. Si, X. Lyu, P.D. Ye, Ferroelectric polarization switching of hafnium zirconium oxide in a ferroelectric/dielectric stack, ACS Appl. Electron. Mater. 1 (5) (2019) 745–751, https://doi.org/10.1021/acsaelm.9b00092.

[73] T. Kim, E.R. Borujeny, I. Sardinero-Meirás, J. Grajal, K.C. Cadien, D.A. Antoniadis, J.A. Del Alamo, AC impedance characteristics of ferroelectric Hf0.5Zr0.5O2: from 1 kHz to 10 GHz, 2023 Int. Electron Devices Meet. (IEDM) (2023) 1–4, https://doi.org/10.1109/IEDM45741.2023.10413871.

[74] S.J. Kim, J. Mohan, H.S. Kim, S.M. Hwang, N. Kim, Y.C. Jung, A. Sahota, K. Kim, H.-Y. Yu, P.-R. Cha, C.D. Young, R. Choi, J. Ahn, J. Kim, A comprehensive study on the effect of TiN top and bottom electrodes on atomic layer deposited ferroelectric Hf0.5Zr0.5O2 thin films, Materials 13 (13) (2020) 2968, https://doi.org/10.3390/ma13132968.

[75] R. Han, P. Hong, B. Zhang, M. Bai, J. Hou, J. Yang, W. Xiong, S. Yang, J. Gao, Y. Lu, F. Liu, F. Luo, Z. Huo, Understanding the stress effect of TiN top electrode on ferroelectricity in Hf0.5Zr0.5O2 thin films, J. Appl. Phys. 134 (19) (2023) 194104, https://doi.org/10.1063/5.0176345.

[76] Y. Goh, J. Hwang, Y. Lee, M. Kim, S. Jeon, Ultra-thin Hf0.5Zr0.5O2 thin-film-based ferroelectric tunnel junction via stress induced crystallization, Appl. Phys. Lett. 117 (24) (2020) 242901, https://doi.org/10.1063/5.0029516.

[77] B.Y. Kim, I.S. Lee, H.W. Park, Y.B. Lee, S.H. Lee, M. Oh, S.K. Ryoo, S.R. Byun, K. D. Kim, J.H. Lee, D.-Y. Cho, M.H. Park, C.S. Hwang, Top electrode engineering for high-performance ferroelectric Hf0.5Zr0.5O2 capacitors, Adv. Mater. Technol. 8 (16) (2023) 2300146, https://doi.org/10.1002/admt.202300146.

[78] M. Su, S. Gao, Z. Weng, L. Zhao, C. Lee, Y. Zhao, Improvement of ferroelectricity and reliability in Hf0.5Zr0.5O2 thin films with two-step oxygen vacancy engineering, IEEE Electron Device Lett. 43 (7) (2022) 1057–1060, https://doi.org/10.1109/LED.2022.3179489.

[79] D.R. Islamov, T.M. Zalyalov, O.M. Orlov, V.A. Gritsenko, G. Krasnikov, Ya. Impact of oxygen vacancy on the ferroelectric properties of lanthanum-doped hafnium oxide, Appl. Phys. Lett. 117 (16) (2020) 162901, https://doi.org/10.1063/5.0023554.

[80] J. Petzelt, Dielectric grain-size effect in high-permittivity ceramics, Ferroelectrics 400 (1) (2010) 117–134, https://doi.org/10.1080/00150193.2010.505511.

[81] N. Setter, D. Damjanovic, L. Eng, G. Fox, S. Gevorgian, S. Hong, A. Kingon, H. Kohlstedt, N.Y. Park, G.B. Stephenson, I. Stolitchnov, A.K. Taganstev, D. V. Taylor, T. Yamada, S. Streiffer, Ferroelectric thin films: review of materials, properties, and applications, J. Appl. Phys. 100 (5) (2006) 051606, https://doi.org/10.1063/1.2336999.